(gradual softening) branches.

Measurement of load-shear displacement curve--On the other hand, the relation between load and shear displacement at load end can be also used to identify the local $\tau-\delta$ relation if the shape such as the ones shown in Fig. 4 is assumed a priori. The load-shear displacement relation at loading end as shown in Fig. 16 may be measured directly with the help of clip gauge (Fig. 3). Moreover, it can be also obtained through the measurement of FRP strain distribution for whole loading steps, where the shear displacement can be calculated through the integration of strain distribution along FRP laminate. Fig. 16 shows some special points such as occurrence of micro debonding (A), occurrence of macro debonding (B) and occurrence of final debonding failure (C). Both points (a) ($u_1$, $P_1$) and (B) ($u_2$, $P_{max}$) can be considered to correspond to the ones ($\delta_1$, $\tau_{max}$) and ($\delta_f$, 0) in $\tau-\delta$ curve. Therefore, the following expressions can be obtained easily.

$$\delta_f = u_2,\quad \tau_f = \frac{P_{max}^{\;2}}{E_1 t_1 b_1^{\,2} u_2},\quad \delta_1 = u_1 \text{ or } \delta_1 = \frac{P_1^2}{E_1 t_1 b_1^{\,2} \tau_f} \tag{13}$$

A redundant equation can be used to verify the accuracy. After occurrence of macro debonding, the interfacial cracking starts to propagate to the FRP end. Theoretically, there is no loading increase or decrease during the debonding propagation from (B) to (C). However, due to the heterogeneities along the FRP-concrete interface, both case 1 and case 2 as shown in Fig. 16 is observed in the experiment. Fig. 17 shows the identified result for the specimen S-CFS-400-25, i.e. $\delta_1 = 0.1\,\text{mm}$, $\delta_f = 0.3\,\text{mm}$, $\tau_f = 8\,\text{MPa}$. The load-shear displacement curve calculated theoretically based on the identified parameters is also shown in Fig. 17 for comparison with the ones based on measurement of clip gauge and strain gauge of FRP strain distribution. The $\tau-\delta$ relation identified by this kind of approach is considered to be more practical.

## CONCLUSIONS

From both experimental and analytical studies on bond properties of FRP laminates the following conclusions are obtained

1) Through the experimental program using both single-lap shear test specimens and double-lap shear test specimens designed to study the interfacial behavior of FRP-concrete interface, the load-carrying capacity, FRP strain distribution, interfacial shear stress distribution and effective stress transfer length affected by the equivalent stiffness of FRP laminates are quantitatively discussed.

2) The nonlinear relationships derived for some typical local shear-deformation curves with and without softening behavior are used to discuss the shear stress transfer and fracture propagation behavior by comparing with experimental findings. It is found that the ascending and descending model gives more close simulation for both interfacial shear stress distribution and effective stress transfer length.

3) Through the comparison between experimental and theoretical results, the interfacial fracture energies are quantitfied.

4) The two methods to determine the local shear stress-displacement relationship are discussed, based on the following experimental results, respectively: a) Load-shear displacement relation at loading end; b) FRP strain distribution, through which the local shear-displacement curve can be obtained from the relationship of shear stresses varying with locations along the interface at a given appropriate loading step or with loading step at a given appropriate locations. The identified results by method a) is considered to be practical.

## REFERENCES


(1) Täljsten, B.: Strengthening of concrete prisms using the plate-bonding technique, I. J. of Fracture, Vol. 82, 253-266, 1996.

(2) Brosens, K. and Gemert, D. V.: Plate end shear design for external CFRP laminates, Fracture Mechanics of Concrete Structures, Proceedings FRAMCOS-3, AEDIFICATIO Publishers, D-79104 Freiburg, Germany, 1793-1804, 1998.

(3) Wu, Z. S., and Niu, H. D.: Study on debonding failure load of RC beams strengthened with FRP sheets, J. of Structural Engineering, JSCE, 46A, 2000(to be appeared).

(4) Wu, Z. S. and Yoshizawa, H.: Analytical/Experimental study on composite behavior in strengthening structures with bonded carbon fiber sheets, J of Reinforced Plastics and Composites, Vol. 18(2), 1131-1155, 1999.

(5) Yin, J. and Wu, Z. S.: Interface crack propagation in FRP-strengthening structures using nonlinear fracture mechanics, 4th International Symposium on Fiber Reinforced Polymer for Reinforced Concrete Structures, SP-188, ACI International, Baltimore, Oct. 31-Novem. 5, 1999, 1035-1047.

(6) Yuan, H., Wu, Z. S. and Yoshizawa, H.: Theoretical solutions on interfacial stress transfer of externally bonded steel/composite laminates, J. of Structural Mechanics and Earthquake Engineering, JSCE, (to be appeared).

(7) Chajes, M. J., Finch, W. W., Januszka, T. F. and Thomson, T. A.: Bond and force transfer of composite material plates bonded to concrete, ACI Structural J., Vol. 93(2), 208-217, 1996.

(8) Ueda, T., Sato, Y. and Asano, Y.: Experimental study on bond strength of continuous carbon fiber sheet, 4th International Symposium on Fiber Reinforced Polymer for Reinforced Concrete Structures, SP-188, ACI International, Baltimore, 407-416, 1999.

(9) Kamiharaka, A., Shimomura, T., Marurama, K. and Nishida, H.: Stress transfer and peeling-off behavior of continuous fiber reinforced sheet-concrete system, Symposium of EASEC-7, Kochi, Japan, 1283-1288, 1999.

(10) Wu, Z. S., Murayama, D. and Yoshizawa, H.: An experimental study on bonding behavior and its improvement approach of CFRP sheets in anchorage zone, Proceedings of the Japan Concrete Institute, Vol. 21(2), 211-216, 1999.

TABLES

**Table 1** Mechanical properties of FRP laminates and concrete

| Materials | | Specific Characteristics | Properties | Fiber Arial weight g/m$^2$ | Design Thickness mm |
|---|---|---|---|---|---|
| Concrete | | Comp. Strength (Single-lap Shear Test) | 57.6 MPa | - | - |
| | | Comp. Strength (Double-lap Shear Test) | 42.0 MPa | - | - |
| Carbon Fiber Sheet | HT | Young's Modulus | 230 GPa | 150 | 0.083 |
| | | Tensile strength | 4.2 GPa | 200 | 0.111 |
| | | | | 300 | 0.167 |
| | HM | Young's Modulus | 390 GPa | 300 | 0.167 |
| | | Tensile strength | 4.4 GPa | | |
| PBO Fiber Sheet | HM | Young's Modulus | 270 GPa | 200 | 0.128 |
| | | Tensile strength | 4.5 GPa | | |
| Carbon Fiber Plate | HT | Young's Modulus | 138 GPa | 1100 | 1.0 |
| | | Tensile strength | 2.52 GPa | 2200 | 2.0 |

**Table 2** Specimens used for shear tests

(a) Double-lap shear test

| Quality of FRP laminate | Stiffness of FRP kN/mm | Fiber Arial weight g/m$^2$ | Concrete Surface Preparation | Bond Length L mm | No. of Specimens |
|---|---|---|---|---|---|
| HT Carbon Fiber Sheet | 19.1 | 150 | Diamond sander/putty | 300 | D-CFS-150-30 |
| | 38.4 | 300 | same | 300 | D-CFS-300-30 |
| | 76.8 | 600 | same | 300 | D-CFS-600-30 |
| HM Carbon Fiber Sheet | 64.4 | 300 | same | 300 | D-CFM-300-30 |
| Aramid Fiber Sheet | 23.9 | 280 | same | 300 | D-AR-280-30 |

(b) Single-lap shear test

| Quality of CFS | Stiffness of CFS kN/mm | Fiber Arial weight g/m$^2$ | Concrete Surface Preparation | Bond Length L mm | No. of Specimens |
|---|---|---|---|---|---|
| HT Carbon Fiber Sheet | 51.1 | 400 | Diamond sander/putty | 250 | S-CFS-400-25 |
| HM Carbon Fiber Sheet | 64.4 | 300 | same | 250 | S-CFM-300-25 |
| | 193.1 | 900 | same | 250 | S-CFM-900-25 |
| HM PBO Fiber Sheet | 34.6 | 200 | same | 250 | S-PBO-200-25 |
| HT Carbon Fiber Plate | 138.0 | 1100 | same | 250 | CP1-L25 |
| | 276.0 | 2200 | same | 250 | CP2-L25 |

**Table 3** Shear test results

(a) Double-lap shear test

| Quality of FRP laminate | Stiffness of FRP kN/mm | Bond Length L mm | Specimens | No. of Specimen | Max. Load kN | Max. Debonding Load kN/cm | Failure Mode |
|---|---|---|---|---|---|---|---|
| HT | 19.1 | 300 | D-CFS-150-30 | 1 | 24.4 | 2.44 | Debonding |
| HT | | | | 2 | 23.6 | 2.36 | Debonding |
| HT | | | | 3 | 24.5 | 2.45 | Debonding |
| | | | | Av. | 24.1 | 2.41 | - |
| | 38.4 | 300 | D-CFS-300-30 | 1 | 37.8 | 3.78 | Rupture of FRP |
| | | | | 2 | 33.9 | 3.39 | Debonding |
| | | | | 3 | 33.3 | 3.33 | Debonding |
| | | | | Av. | 35.0 | 3.50 | - |
| | 76.8 | 300 | D-CFS-600-30 | 1 | 51.3 | 5.13 | Debonding |
| | | | | 2 | 50.7 | 5.07 | Debonding |
| | | | | 3 | 54.5 | 5.45 | Debonding |
| | | | | Av. | 52.1 | 5.21 | - |
| HM Carbon Fiber | 64.4 | 300 | D-CFM-300-30 | 1 | 39.0 | 3.90 | Rupture of FRP |
| | | | | 2 | 39.0 | 3.90 | Debonding |
| | | | | 3 | 32.5 | 3.25 | Rupture of FRP |
| | | | | Av. | 36.8 | 3.68 | - |
| Aramid Fiber | 23.9 | 300 | D-AR-280-30 | 1 | 25.5 | 2.55 | Debonding |
| | | | | 2 | 25.7 | 2.57 | Debonding |
| | | | | 3 | 23.8 | 2.38 | Debonding |
| | | | | Av. | 25.0 | 2.50 | - |

(b) Single-lap shear test

| Quality of FRP Laminate | Stiffness of FRP kN/mm | Bond Length L mm | Specimens | No. of Specimen | Max. Load kN | Max. Debonding Load kN/cm | Failure Mode |
|---|---|---|---|---|---|---|---|
| HT Carbon Fiber Sheet | 51.1 | 250 | S-CFS-400-25 | 1 | 15.4 | 3.84 | Debonding |
| | | | | 2 | 13.9 | 3.48 | Debonding |
| | | | | 3 | 13.0 | 3.25 | Debonding |
| | | | | Av. | 14.1 | 3.52 | - |
| HM Carbon Fiber Sheet | 64.4 | 250 | S-CFM-300-25 | 1 | 12.0 | 3.01 | Debonding (within adhesive) |
| | | | | 2 | 11.9 | 2.97 | Debonding (within adhesive) |
| | | | | Av. | 12.0 | 2.99 | - |
| | 193.1 | 250 | S-CFM-900-25 | 1 | 25.9 | 6.48 | Debonding |
| | | | | 2 | 23.4 | 5.85 | Debonding |
| | | | | 3 | 23.7 | 5.92 | Debonding |
| | | | | Av. | 23.5 | 5.88 | - |
| HM PBO Fiber Sheet | 34.6 | 250 | S-PBO-200-25 | 1 | 14.3 | 3.56 | Debonding |
| | | | | 2 | 12.2 | 3.04 | Debonding |
| | | | | Av. | 13.2 | 3.30 | - |
| HT Carbon Fiber Plate | 138.0 | 250 | CP1-L25 | 1 | 16.99 | 3.40 | Debonding |
| | | | | 2 | 16.96 | 3.39 | Debonding |
| | | | | 3 | 17.23 | 3.45 | Debonding |
| | | | | Av. | 17.06 | 3.41 | - |
| | 276.0 | 250 | CP2-L25 | 1 | 22.32 | 4.46 | Debonding |
| | | | | 2 | 23.69 | 4.74 | Debonding |
| | | | | 3 | 23.11 | 4.62 | Debonding |
| | | | | Av. | 23.04 | 4.61 | - |

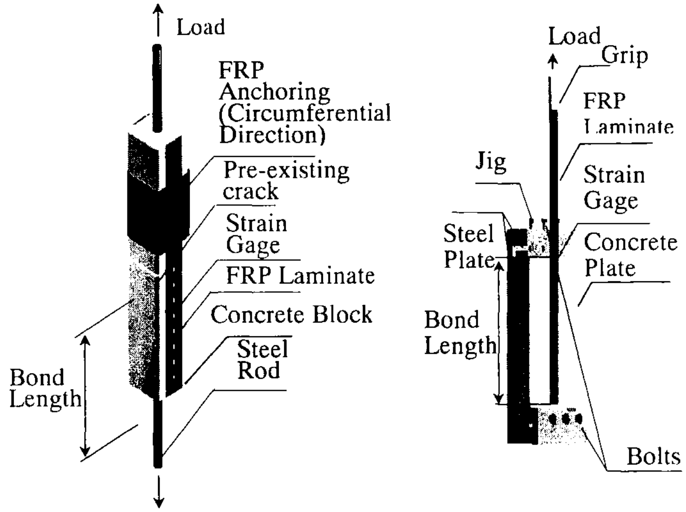


(a) Double-lap shear test (b) Single-lap shear test

Fig. 1. Experimental methods

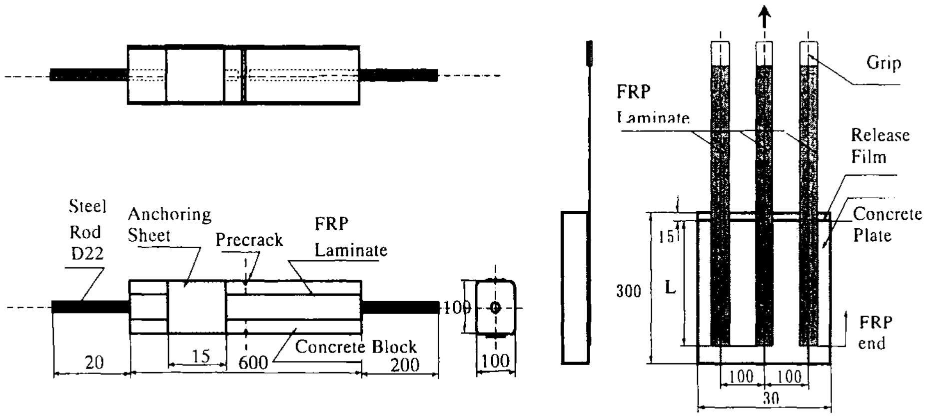


(a) Double-lap shear test (b) Single-lap shear test

Fig. 2. Specimen configuration

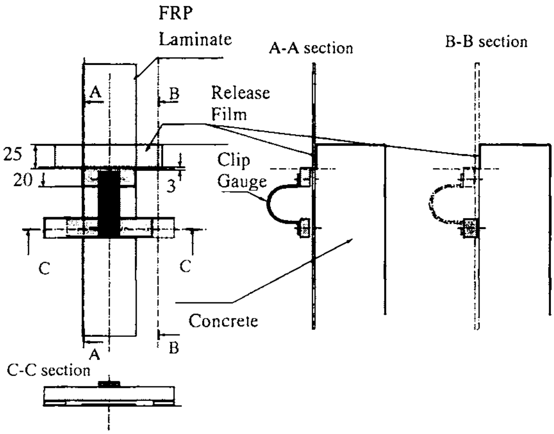


Fig. 3. Measurement of relative shear displacement

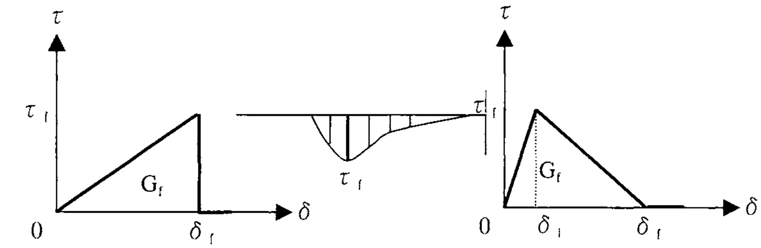


(a) Linear ascending branch (model I)

(b) Linear ascending and descending branches (model II)

Fig. 4. Simplified local shear stress-slip relations

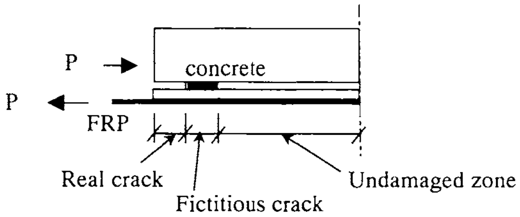


Fig. 5. Fictitious crack model and shear stress distribution

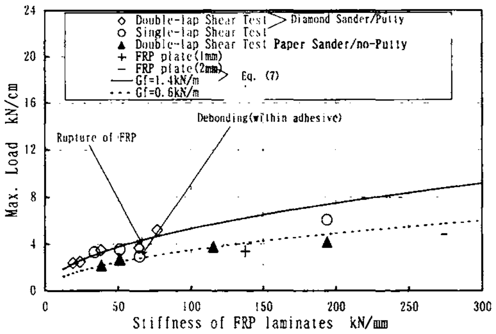


Fig. 6. Relationship between load-carrying capacity and FRP stiffness

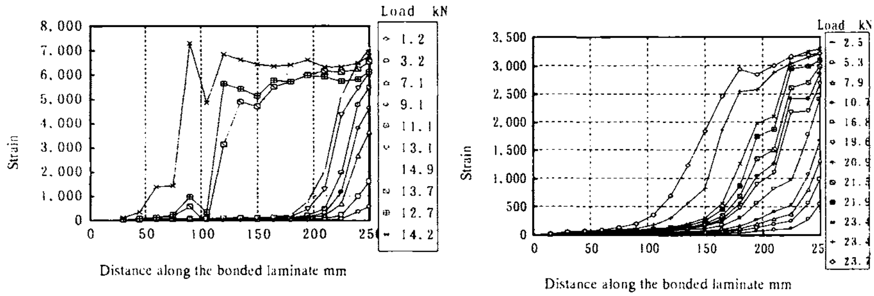


(a) S-CFS-400-25 (b) S-CFM-900-25

Fig. 7. Examples of strain distribution in FRP laminate

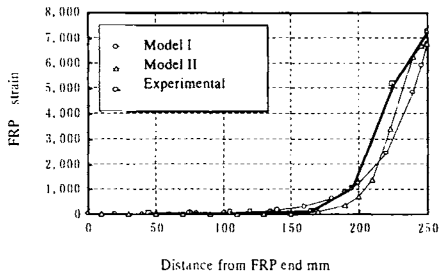


Fig. 8. Comparison of experimental and theoretical FRP strain distribution

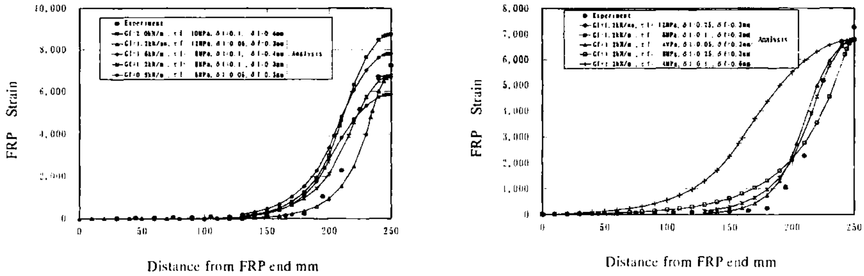


(a) S-CFS-400-25 (b) S-CFS-400-25 ($G_f$=1.2kN/m)

Fig. 9. Identification of FRP strain distribution

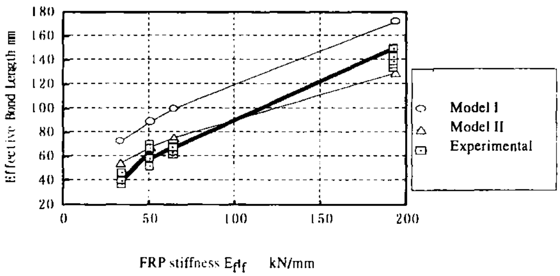


Fig. 10. Comparison of experimental and theoretical results on effective stress transfer length

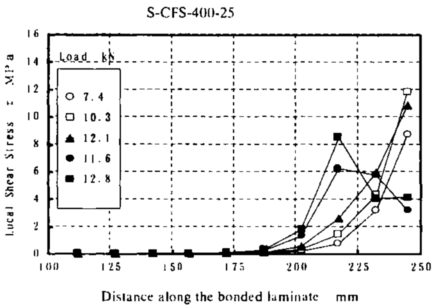


Fig. 11. Experimental results on local shear stress distribution

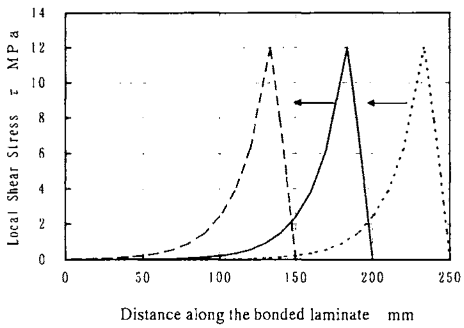


Fig. 12. Shear stress distribution due to crack propagation (theoretical value)

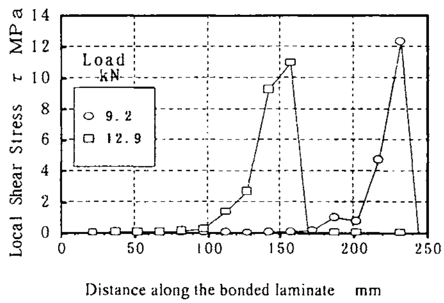


Fig. 13. Shear stress distribution due to crack propagation (experimental value)

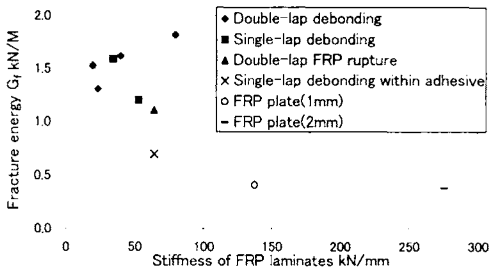


Fig. 14. Identified results of interfacial fracture energy